

Variability of the Indian Ocean SST and Its Impacts on Asian-Australian Monsoon Climate

SOO-HYUN YOO

School of Earth and Environmental Sciences, Seoul National University, Seoul 151-742, Korea

RSIS, Climate Prediction Center, NCEP/NWS/NOAA, Camp Springs, Maryland, USA

SONG YANG

Climate Prediction Center, NCEP/NWS/NOAA, Camp Springs, Maryland, USA

CHANG-HOI HO

School of Earth and Environmental Sciences, Seoul National University, Seoul 151-742, Korea

October 2005

Accepted by *Journal of Geophysical Research*

Corresponding author address: Miss Soo-Hyun Yoo, RSIS, Climate Prediction Center, NCEP/NWS/NOAA, 5200 Auth Road, Rm 800, Camp Springs, MD 20746. Email: soohyun.yoo@noaa.gov

Abstract

In this study, the authors investigate the relationships between the Indian Ocean (IO) sea surface temperature (SST) and the Asian-Australian monsoon (AAM) on seasonal to interannual timescales. They focus on the dominant features of IO SST, the impacts of IO SST on different monsoon components, and the relative importance of the northern and southern IO for the AAM.

The dominant mode of IO SST is often characterized by uniform warming or cooling, with maximum variance in the southern hemisphere. This mode exerts a larger impact on monsoon variability than does the tropical IO dipole. The IO SST is strongly persistent from the boreal fall to the next spring even summer and less persistent from boreal summer to fall, a feature related to seasonal alternation of the dominance of the impacts of Pacific and IO SSTs on the Asian-Australian monsoons. While the tropical central Pacific SST exerts an apparently larger impact on the monsoon climate in the boreal winter and the transitional seasons, the IO SST affects the summer regional climate more strongly. The springtime IO SST leads to opposite changes in the South Asian monsoon (SAM) and the Southeast Asian monsoon (SEAM), reinforcing the out-of-phase relationship that appears often between the two monsoon components. While a warmer IO strengthens the SAM, it weakens the SEAM. Furthermore, the southern IO SST is related to the Asian summer monsoon more closely than the northern IO SST. The boreal fall IO SST, especially that in the north IO, is strongly associated with the subsequent Australian summer monsoon.

1. Introduction

The Indian Ocean (IO) is a place of substantial interest in climate studies because its sea surface temperature (SST) plays an important role in determining many climate features. The variability of IO SST, which is characterized by a strong annual cycle, particularly in the northern IO, is linked to the variability of monsoons in Asia, Australia, and Africa. The variability of IO SST is also associated with El Niño/Southern Oscillation (ENSO), which significantly regulates the global climate.

A number of pioneering studies [e.g., Saha 1970; Shukla, 1975; Shukla and Misra 1977] sought to understand the forcing-and-response aspect of the relationship between IO SST and the Indian monsoon and to seek predicative information for the monsoon despite the scarcity of reliable observations and numerical models. However, it was found that the SST-monsoon relationship was complex, which hindered skillful prediction of the monsoon using IO SST. Indeed, the fluctuation of IO SST and its relationship with monsoon depend, in part, on the air-sea interaction that takes place when the monsoonal flow occurs over the Arabian Sea and the Bay of Bengal [also see Druyvan et al., 1983; Rao and Goswami, 1988; Harzallah and Sadourny, 1997].

There exists substantial debate regarding the role of IO SST in monsoon variability. While some experiments with general circulation models show that Pacific SST alone generates monsoon anomalies similar to observed, others indicate that the variability of IO SST causes significant

changes in the Indian monsoon [e.g., Zhu and Houghton, 1996; Terray et al., 2003, 2005] thus de-emphasizing the role of IO SST [Palmer et al., 1992; Chen and Yen, 1994]. Perhaps the strongest interannual relationship between IO SST and the Indian monsoon has been found on the biennial timescale, as shown by studies of the tropospheric biennial oscillation [TBO; Meehl, 1987, 1997; Chang and Li, 2000; Kim and Lau, 2001; Meehl and Arblaster, 2002]. In the context of TBO, a warming in IO increases the Indian summer monsoon, which leads to a strong Australian monsoon in the subsequent boreal winter. Using a coupled atmosphere-ocean general circulation model, Yu et al. [2003] verified that the Indian Ocean plays a more critical role than the Pacific Ocean in the TBO transition from a strong (weak) Australian monsoon to a weak (strong) Indian summer monsoon.

In the last decade, the Indian Ocean Dipole [IOD; Saji et al., 1999; Webster et al., 1999] has generated considerable interest in IO studies. It has been claimed that the dipole influences the climate of East Africa and Indonesia [Saji et al., 1999], South Asia [Ashok et al., 2001], East Asia [Saji and Yamagata, 2003; Guan and Yamagata, 2003], the Mediterranean, Australia, and even Brazil [Ashok et al., 2003a; Saji and Yamagata, 2003]. In some studies, the IOD is considered a local ocean-atmosphere coupled phenomenon, whose evolution is mostly independent from the Pacific influence [e.g. Behera et al., 1999; Saji et al., 1999; Webster et al., 1999; Rao et al., 2002; Yamagata et al., 2002; Ashok et al., 2003b; Yu et al., 2003; Shinoda et al., 2004; Yu and Lau,

2004]. However, other studies have shown a strong relationship between IOD and ENSO [e.g., Murtugudde et al., 2000; Allan et al., 2001; Baquero-Bernal et al., 2002; Dommenges and Latif, 2002; Xie et al., 2002; Krishnamurthy and Kirtman, 2003].

Several studies have also explored the climate impact of southern IO SST. For example, observational and numerical studies have revealed a positive relationship between extratropical IO SST and African rainfall (e.g., Mason, 1995; Reason, 1998, 2001, 2002; Goddard and Graham, 1999; Behera and Yamagata, 2001). Nicholls [1989] and Drosowsky and Chambers [2001] showed that the southern Indian Ocean SST influences the Australian rainfall. Using an atmospheric general circulation model, Zhu and Houghton [1996] found that the variability of Asian summer monsoon is sensitive to the conditions of SST in the tropical southern IO. Recently, Terray et al. [2003] found that the southeast IO SST during boreal winter, when linked to the subtropical IO dipole pattern described by Behera and Yamagata [2001] and to ENSO, is a major precursory signal for the Indian summer monsoon. In a follow-up study, Terray et al. [2005] emphasized the importance of the southern IO for an ENSO-monsoon relationship. They further emphasized the role of southeastern IO SST in maintaining the overlying atmospheric circulation pattern, which interacts with ENSO and convection over the maritime continent and, in turn, maintains the existing SST anomalies. According to White and Peterson [1996] and Peterson and White [1998], the anomalies in the extratropical IO and the overlying atmosphere are related to the

Antarctic circumpolar wave. However, as discussed by Behera and Yamagata [2001], the role of external forcing such as ENSO through the atmospheric and/or oceanic processes in extratropical IO variability should not be excluded.

In brief, the IO SST is often believed to play an important role in influencing the Asian-Australian monsoon (AAM), especially on the biennial timescale. However, many questions regarding the climate impact of IO SST remain unanswered. For example, what are the different climate impacts of the IOD and the dominant mode of IO SST? What are the relative influences of the northern IO and the southern IO on the AAM? Does the IO SST affect the different Asian monsoon components selectively?

In this study, we address the above questions regarding the relationships between the Indo-Pacific SST and the Asian-Australian monsoons. We focus on the importance of the seasonal evolutions of SST and the atmospheric circulation, especially the difference in the phase-locking of SST persistence between IO and the Pacific, for explaining the interrelated features of SST and monsoon climate. We also focus on the differences associated with different monsoon components and on the relative importance of the northern and southern IO.

In section 2, we provide a description of the data sets and analysis methods used in this study. Features of the dominant modes of IO SST are presented in section 3. In sections 4 and 5, we

discuss the simultaneous SST-monsoon relationship and the predictive potential of IO SST. Finally, a summary of the main findings and further discussions of the results are given in section 6.

2. Data and analysis methods

a. Data

The primary datasets used in this study include three widely-used products. They are the National Centers for Environmental Prediction (NCEP) - National Center for Atmospheric Research (NCAR) global reanalysis [Kalnay et al., 1996], NCEP's Optimally Interpolated SST [Reynolds et al., 2002], and NOAA's Climate Prediction Center Merged Analysis of Precipitation [CMAP; Xie and Arkin, 1996].

The SST data set provides weekly information of 1° (longitude and latitude) resolution, covering the time period from 1981 to present. Even though other datasets such as the NCEP extended reconstructed SST provide longer data records, we chose the optimally interpolated SST for several reasons. First, there is a relative homogeneity of data sources (satellites and *in situ*) and analysis techniques for the data period. Second, the chosen SST data is available at latitudes poleward of 45°S , which is necessary for studying the climate impact of the extratropical IO. Third, there exists a potential problem in the NCEP-NCAR reanalysis in its early years for studying the Asian monsoon because of an encoding error that may have caused a discontinuity in data quality

over some Asian regions before and after 1968 [Yang et al., 2002]. Fourth, the CMAP precipitation is available since 1979. These problems in data quality and availability hinder the application of earlier SST in our study. In fact, analyzing the period of optimally interpolated SST prevents discussion of the interdecadal variability, because abrupt climate change occurred in the mid-1970s [Nitta and Yamada, 1989; Ashok et al., 2004a]. However, this is not a focus of this study.

The other datasets used in this study include the all-India monsoon rainfall (AIMR) index, which is an areal average of rainfall in India's 29 meteorological subdivisions [Parthasarathy et al., 1995]. Rainfall amounts are the totals for June, July, August, and September and AIMR index is available online at <http://grads.iges.org/india/allindia.data>. We also use the IOD index [Saji et al., 1999], available online at <http://www.jamstec.go.jp/frsgc/research/d1/iod> and the NINO3 SST over the tropical central-eastern Pacific (5°S - 5°N , 90°W - 150°W).

b. Analysis methods

We apply an empirical orthogonal function (EOF) analysis to identify the leading patterns of IO SST variability. We also apply a singular value decomposition (SVD) analysis to depict the relationship between IO SST and large-scale precipitation and circulation patterns. For this, we applied the method of Bretherton et al. [1992] to examine the heterogeneous regression patterns of the dominant SVD modes. The main features of this method will be discussed in section 5. In

addition, linear correlation and regression analyses are generated, and the 2-tailed Student's t -test is used to determine the statistical significance of the results.

3. Dominant features of IO SST variability

To understand the variability of IO SST, we focus on the locations of large SST fluctuations, the dominant modes of SST variability, and the extratropical southern IO. Figure 1 shows the climatology and tendency of seasonally-averaged SST. In December-February (DJF; Figure 1a), the SST over 28°C spreads zonally between 15°S and 10°N, with the warmest areas to the north of Australia and west of Sumatra. The SST tendency from September-November (SON) through December-February (DJF) is negative in the northern hemisphere and positive in the southern hemisphere, with the maximum increase in SST (>4.5°C) occurring between 30°S and 40°S. In March-May (MAM; Figure 1b), the IO SST reaches its maximum in the equatorial and northern IO. From DJF to MAM, SST varies little in the southern IO. However, from MAM to June-August (JJA; Figure 1c), SST decreases in the entire IO, although JJA is still the season of second highest SST in the northern IO. The cooling in the southern IO suggests a strong local annual cycle, given the maximum SST increase from SON to DJF (see Figure 1a). The cooling in the northern IO is caused by the activity of the Asian monsoon. Note that the highest IO SST in JJA appears near the equator, except over the western ocean because of the upwelling associated with the Somali current.

From JJA to SON, the IO SST changes are relatively small (Figure 1d). As a seasonal transition, the tropical northern IO SST decreases slightly; however, the western IO SST increases because of the weakened monsoon flow. These changes in SST also explain why the IOD is most prominent in SON as the annual cycle augments the zonal gradient in SST in boreal fall.

We now describe the interannual variability of IO SST and its relationship with atmospheric circulation patterns. Figure 2 shows SST standard deviations and 850-mb climatological winds. We superimpose the two fields in the figure to facilitate the discussion of atmospheric background features associated with SST variability. In DJF and MAM (Figures 2a-b), the largest standard deviations of SST occur in the southern IO, associated with an overlying anticyclonic circulation and westerly flow on its southern flank. Maximum SST variability appears in DJF when the anticyclonic pattern is strongest. In JJA (Figure 2c), the largest SST variability is located in the tropical western IO and off Sumatra due to the coastal air-sea interaction associated with monsoon activity, and in the extratropical southern IO related to the overlying westerlies. In SON (Figure 2d), the largest standard deviations of SST emerge from the eastern center of IOD (off Sumatra). However, the SST variability in the western center of IOD is much weaker. While the withdrawal of the Indian summer monsoon reduces SST variability in the northern IO, standard deviations in the southern IO are similar between JJA and SON.

To understand the features related to the dominant modes of IO SST variability, we also

generate an EOF analysis for each season and for the domain of 60°S-30°N, 50°E-110°E. Figure 3 shows the regression of grid-point SST against the first principal component of the EOF (EOF1) for IO SST. In the figure, the filled arrows illustrate the evolution of IO SST while the non-filled arrows estimate the lag relationships between IO and NINO3 SSTs. The lag-relationships will be discussed in more detail in section 5. Figure 3 indicates that the dominant modes are often associated with relatively uniform warming or cooling in IO. In DJF, a center of maximum SST variation appears over the subtropical southern IO. In MAM, a dipole-like pattern emerges between the northeastern and southwestern IO, although uniform SST variability appears across most of the IO. The southwestern center, which is weaker in other seasons, is the location of large SST variability underneath the extratropical westerlies (see Figure 2b). According to An [2004], the basin-wide warming north of 20°S in spring is primarily caused by ENSO, and is indicated by an increase in heat content associated with the surface easterly wind over the western IO and an increase in solar radiation associated with the suppressed convection via an atmospheric bridge over the eastern IO. When IO SST varies strongly with the Asian monsoon flow (JJA), a uniform warming/cooling SST pattern appears over the northern IO and large SST variation associated with the Somali jet appears over the western IO. In SON, SST variability with an opposite sign occurs off Sumatra. Large-scale warming/cooling and the tropical IOD appears most clearly in this season (SON). (A dipole-like pattern of SST in the eastern center of IOD and the central southern IO is

also prominent in SON.). While it is known that results from EOF analysis are often domain dependent [see Dommenges and Latif, 2002; Behera et al., 2003], we have confirmed the features shown in Figure 3 by performing the analysis for different ocean domains including an extension of the western boundary to 30°E. Indeed, the features remain largely unchanged unless the analysis domain is extended well into the Pacific Ocean.

The variability of eastern IO SST is strongly associated with changes in convective activity over the maritime continent [Wang et al., 2003]. The atmospheric Rossby wave response to a reduction in the convection generates an anticyclonic pattern over the tropical eastern IO, which causes oceanic cooling off Sumatra in summer and fall. Toward winter, this cooling becomes weaker and even disappears as the basic flow changes from southeasterly to northwesterly leading to a uniform SST pattern [Li et al., 2003]. In addition, the effect of ENSO, which is usually strongest in DJF, also contributes to the relatively uniform pattern of IO SST via the atmospheric “bridge” [Lau and Nath, 1996; Alexander et al., 2002]. More discussion about these seasonally dependent features and their association with AAM are given in the next two sections.

4. Simultaneous IO SST and monsoon relationships

Figure 4 shows the patterns of regression of 850-mb winds and precipitation against the leading EOF mode for each season. As seen in Figure 4a, the DJF EOF1 is associated with an

anomalous anticyclone over the western North Pacific, centered over the Philippine Sea. Connected to this circulation pattern are significant easterly wind anomalies over the equatorial IO, which implies a weaker westerly basic flow. Correspondingly, precipitation decreases over the eastern IO, especially west of Sumatra, in the western Pacific Ocean, and to the north of Australia. Over eastern Africa and the equatorial western IO, precipitation increases, partially associated with weaker upwelling caused by intensification of easterly flow over the tropical IO. Figure 4a also reveals that the anomalous northwesterly winds weaken the prevailing climatological southeasterlies over the southeastern IO, leading to warming in the ocean domain because the wind-evaporation feedback reduces the latent and sensible heat release from the ocean surface.

In MAM (Figure 4b), the leading SST mode is associated with anomalous easterly flow over the equatorial IO, anomalous convergence over the equatorial western IO, and a weakening of an anticyclonic circulation over the southern IO. These changes cause an increase in precipitation over the tropical western IO due to convergence, with anomalous westerly flow near the east of Africa and over the west of Australia by wind-evaporation-SST feedback through the weakening of an anticyclonic circulation (Li et al., 2003; Terray et al., 2003; Fischer et al., 2005). In addition, precipitation increases over East Asia and decreases over Southeast Asia, in a manner consistent with the changes in the atmospheric circulation.

The JJA EOF1 is linked mainly to changes in the Asian monsoon (Figure 4c). Over the

Arabian Sea, a warming of SST is accompanied by a weakening of the monsoon flow. The most significant signal appears over Southeast and East Asia, associated with the intensification and northwestward expansion of the subtropical western Pacific high. These changes in the subtropical high weaken the monsoon flow over the South China Sea, decrease the precipitation over the Philippines, and shift the rain band northward to Korea and Japan.

In SON (Figure 4d), significant large-scale signals appear over IO and the western Pacific, including the intensifying southeasterly basic flow near Sumatra, the weakening of westerly basic flow over tropical western IO, and a climatic cyclonic circulation over the South China Sea. These signals are consistent with the broad-scale warming in the western IO and the cooling west of Sumatra. The cooling west of Sumatra is also connected to the anticyclonic anomaly over southeastern IO and Southeast Asia, resulted from the Rossby wave response to the weakened convection over the maritime continent [Annamalai et al., 2003; Li et al., 2003]. Correspondingly, precipitation decreases over the eastern IO and Southeast Asia and increases over the western IO. It should also be pointed out that the precipitation and atmospheric circulation patterns are more similar to those associated with IOD in SON than in other seasons.

To verify the features shown in Figure 4, we reveal the linkages between the dominant mode of IO SST and climate phenomena such as the various monsoon components, ENSO, IOD, and the subtropical dipole pattern (SDP; Behera and Yamagata, 2001). The monsoon components

are the AIMR, Webster-Yang large-scale monsoon [WY; Webster and Yang, 1992], South Asian monsoon [SAM; Goswami et al., 1999], East Asian monsoon [EAM; Lau et al., 2000], Southeast Asian monsoon [SEAM; Wang and Fan, 1999], and Australian monsoon [Meehl and Arblaster, 2002]. The definitions of the various monsoon components and SST indices are summarized in Table 1. In particular, WY, SAM, SEAM, and EAM are dynamical monsoon indices, and AIMR and Australian monsoon index are defined by area averages of rainfall. It should be pointed out that the present study only focuses on the Australian summer (DJF) monsoon, which is measured by heavy DJF precipitation over Indonesian and northern Australia (20°S-5°N, 100°-150°E) which are characterized by heavy climatological monsoon rainfall [Nicholls, 1989; Yu et al., 2003]. The Australian monsoon index has also been used in several previous studies, especially related to TBO [Meehl and Arblaster, 2002; Meehl et al., 2003; Yu et al., 2003, Terray et al., 2005]. However, the index examined here may not be suitable for studying the variability of heavy precipitation over eastern Australia.

Table 2 shows the simultaneous correlations between the various indices described in Table 1 and IO SST EOF1, EOF2, and IOD, respectively for each season. Only the values that exceed significance at the 95% confidence level are shown. In DJF, the IO SST EOF1 is significantly correlated with NINO3 SST, IOD, SDP, and the Australian monsoon. There is also a strong relationship between the EOF1 and SDP in MAM. During JJA, EOF1 is significantly linked to two

monsoon components: WY and SEAM. The significant relationship in SON is found between EOF1 and IOD and between EOF1 and NINO3 SST.

In Table 2, we also present the results for IO SST EOF2. This second EOF mode is only significantly correlated with the regional features of IO SST (IOD and SDP), but not directly with NINO3 SST, nor any monsoon component. Table 2 shows another important feature: as with EOF2, IOD is not significantly, simultaneously correlated with any monsoon component at the 95% confidence level. We also can not find any significant relationship between DJF IOD and Australian summer (DJF) monsoon at the 95% confidence level, although there is a simultaneous relationship between the IOD events and the winter (JJA) rainfall of western and southern Australia [Ashok et al., 2003]. Note that the results discussed here are based on monsoon indices and do not necessarily contradict the previous results about the impact of IOD on regional precipitation features (Ashok et al., 2004b; Lau and Nath, 2004; Sarkar et al., 2004). It should also be noted that IOD is a phase-locked phenomenon and usually disappears by the year-end [Saji et al., 1999] and that its climate impact during the boreal winter is naturally weak.

Table 2 not only indicates that the IO SST EOF1 has stronger relationships with AAM than EOF2 and IOD, but also suggests that the general climate features associated with the dominant SST mode can be accounted for by specific phenomena in respective seasons. We further examine the latter features by analyzing the regression of winds and precipitation against various climate

indices. Figure 5 shows the patterns of regression of 850-mb winds and precipitation against (a) NINO3 SST, (b) IOD, (c) SDP, and (d) Australian monsoon for DJF (refer to Table 2). Figure 5a reveals several features: the zonal circulation over the tropical Indo-Pacific Ocean becomes weaker when NINO3 SST is warmer and, as a result, precipitation decreases from the eastern IO to the western Pacific and increases over the western IO and central Pacific. An anomalous anticyclonic circulation appears to the north and south of the weakened equatorial flow. There is an obvious similarity between Figure 4a and Figure 5a, but Figure 5a suggests a larger impact of NINO3 SST on the climate outside the Tropics.

Although both IOD and SDP are associated with local features over the tropical southern IO and Southeast Asia, the patterns in Figures 4a, 5b, and 5c differ substantially from each other. It is interesting to note that SDP is linked to larger changes in winds and precipitation over Southeast Asia than the IOD. The weak climate impact of IOD in the boreal winter is naturally consistent with the termination of the seasonally-locked phenomenon, as mentioned above. Furthermore, the features in Figure 5d are similar to those in Figures 4a and 5a, but of opposite signs. Figures 5a and 5d also reflect the well established strong negative relationship between NINO3 SST and the Australian monsoon.

In JJA, the IO SST EOF1 is significantly correlated with the broad-scale Asian monsoon and SEAM, as noted by changes in the monsoonal flow and precipitation over tropical Asia (Figure

6). A strong monsoon, especially SEAM, is characterized by intensified westerlies over tropical Asia and an anomalous cyclonic pattern over East-Southeast Asia and the western Pacific resulting in precipitation increases over Southeast Asia, the western Pacific, and subtropical Asia, and decreases over South Asia, the tropical IO, and extratropical East Asia. Figure 6b shows that SEAM is linked to even more significant and broad signals. This occurs probably because the SEAM index is defined by the lower tropospheric wind but the WY index is dominated by upper tropospheric flow. A comparison between Figure 4c and Figure 6 indicates that the above climate features are similar to those accounted for by IO SST EOF1 (with opposite signs), especially between Figure 4c and Figure 6b, and for the eastern Asian regions.

We have also examined the features for MAM and SON (figures not shown). In MAM, SDP only captures the features over the southern IO shown in Figure 4b. In SON, both NINO3 SST and the IOD are associated with signals in winds and precipitation like those shown in Figure 4d. This feature suggests that IO SST EOF1 and the IOD are less independent from ENSO in SON as compared to other seasons (also see Table 2).

5. IO SST evolution and predictive potential

We now illustrate the time sequence of the persistent IO SST patterns and the relationship between IO SST and NINO3 SST. For this, we refer to Figure 3. The numbers on the filled arrows

in Fig. 3 represent the correlations between the first mode of IO SST (measured by the principal component) of one season and the mode of the preceding season. The numbers next to the non-filled arrows represent the correlations between the IO SST and the preceding NINO3 SST. The IO SST shows significant relationships between one season and the next. There are also significant lag relationships between IO SST and NINO3 SST. However, the IO-Pacific SST correlations are generally weaker, as seen in Figs. 3a-c. The IO SST persistence is especially strong from SON to the JJA of the following year, but is relatively weak from JJA to SON (Fig. 3d).

The large persistence of IO SST from SON to the following MAM and JJA can be attributed to the interaction between IO SST, ENSO, and the overlying atmospheric conditions including the convection over the maritime continent [Annamalai et al., 2003; Li et al., 2003; Wang et al., 2003; Annamalai et al., 2005; Terray et al., 2005]. For example, a reduction (an enhancement) of the monsoon-related convection over the maritime continent in late summer and early fall generates an atmospheric anticyclonic (cyclonic) pattern over the tropical southeastern IO (off Sumatra) as a Rossby response. Superimposition of the anomalous flow over the background flow leads to large-scale warming (cooling), which lasts to the next spring. ENSO is one of the major contributors to persistent convection anomalies over the maritime continent. In JJA, IO SST is strongly affected by the activity of Asian summer monsoon, as discussed by Meehl and Arblaster [2002] and Yu et al. [2003] who indicated that the effect of Indian monsoon on the transitions of IO SST causes small

SST persistence after the monsoon season. Thus, the feature that the persistence of IO SST drops from JJA to SON due to the influence of the Asian monsoon is different from the change in Pacific SST. As discussed by Webster and Yang [1992] and Lau and Yang [1996], the abrupt development of the Asian monsoon in springtime affects the coupled ocean-atmosphere system in the tropical central Pacific and leads to a significant drop in SST persistence from spring to summer.

The above discussion emphasizes the relative importance of IO SST and NINO3 SST for the dynamics of monsoon-ENSO-IO coupling. The difference in the seasonal transitions of IO and Pacific SSTs has an important implication for explaining the impact of the SSTs on regional climate and their seasonality. Figure 7 shows the regression of 850-mb winds and precipitation against the previous-season IO SST (first EOF mode) and NINO3 SST. Figure 7a illustrates that the SON IO SST is accompanied by a low-level anticyclonic circulation over the southern hemisphere and Southeast Asia, leading to anomalous easterly flow over the equatorial IO. The major features in precipitation include the reduction of monsoon rainfall over equatorial Southeast Asia and to the north of Australia. Increases and decreases of precipitation also occur over the west and east centers of the IOD respectively. In particular, the SON IO SST is negatively correlated with the Australian monsoon. Clearly, the signals in Figure 7a are similar those shown in Figure 4a, reflecting the persistence of SST anomalies from SON to DJF. The DJF IO SST is associated with relatively small changes in the 850-mb winds and precipitation during MAM (Figure 7b) over the tropical

southern IO, Southeast Asia, and the western Pacific. Figures 7b and 4b are quite similar, due to the persistence of IO SST from DJF to MAM.

Figure 7c indicates that MAM IO SST is strongly associated with the subsequent Asian summer monsoon. Warm SST leads to a reduction of large-scale monsoon flow, which can also be seen from Table 3 from WY. The negative relationship between MAM SST and JJA WY monsoon, though only moderately significant, is also consistent with the result of Yang et al. [2004] who indicated that an increase in DJF and MAM IO SST enhances the meridional thermal contrast between IO and Eurasia leading to a stronger jet stream over the Middle East followed by a weaker broad-scale monsoon in the summer.

Figure 7c presents more significant changes in the weakening of SEAM, as shown by the anomalous anticyclone and the reduction of precipitation ($R=-0.64$ for SEAM in Table 3), as well as the intensification of the South Asian monsoon (see both SAM and AIMR in Table 3). It is known that SAM and SEAM are often out of phase with each other [Tao and Chen, 1987]. Thus, the IO SST tends to reinforce the out-of-phase relationship between the two monsoon components. This impact of IO SST is different from the influence of ENSO and IOD, because the latter two are associated with a weak in-phase relationship between the two regional monsoons. Hu et al. [2005] also demonstrated the role of ENSO in reinforcing the connection in rainfall variations between South and East Asia.

Weak convection over the IO associated with cool SST often leads to a weak Indian summer monsoon, which is followed by an El Niño event. Also, during an El Niño year, an anticyclonic pattern develops near the Philippine Sea and is associated with weak summer SEAM, which appears one year after a weak Indian monsoon. In addition, due to its weak to strong transitions associated with the El Niño-La Niña cycle, bienniality often appears in the Indian monsoon component [e.g., Fasullo, 2004]. Therefore, the out-of-phase relationship between the Indian monsoon and SEAM would be expected, supporting the results shown in Figure 7c and Table 3. In summary, the significant relationship between MAM IO SST and JJA Asian monsoon shown in Figure 7c manifests a combination of features shown in Figure 3 about the large persistence of IO SST from MAM to JJA and those presented in Figure 4c about the apparent simultaneous relationship between IO SST and the Asian summer monsoon.

It is evident from Figure 7d that the JJA IO SST is not significantly linked to changes in SON winds and precipitation. In spite of the strong simultaneous relationship for SON (see Figure 4d), the small persistence of IO SST from JJA to SON obstructs the predictive potential of JJA SST.

A comparison between Figures 7a-d and Figures 7e-h reveals several important features about the relative impacts of IO SST and NINO3 SST. The signals in Figure 7e are similar, but much stronger than, those shown in Figure 7a, an agreement that not only reflects the strong relationship between IO SST and NINO3 SST for SON (Table 2) and the significant persistence of

both SSTs from SON to DJF (Figure 3), but also indicates a larger climate impact of the NINO3 SST of these seasons, especially over East Asia and the Pacific Ocean.

The winds and precipitation in MAM vary more strongly with the preceding NINO3 SST than with the preceding IO SST (see Figures 7b and 7f). The impact of NINO3 SST, which extends to the IO, is similar to that shown in Figure 7e, with positive NINO3 SST leading to a weakening of both the equatorial westerlies and the tropical-southern IO easterlies. However, it strengthens the anticyclonic pattern over East-Southeast Asia and the western Pacific. NINO3 SST exerts a stronger impact than does IO SST on the subsequent winds and precipitation of the transitional seasons, as also seen from Figures 7d and 7h for the relationship between JJA SST and SON climate signals.

The Asian summer monsoon is more significantly associated with the preceding IO SST than with the preceding NINO3 SST (Figures 7c and 7g). Indeed, the MAM NINO3 SST is not accompanied by many significant wind and precipitation features over the IO, Asia, and Australia. (An anomalous anticyclonic circulation pattern occurs over the western Pacific.) This result is consistent with that of Webster and Yang [1992] who indicated that, even if the summertime ENSO is perfectly correlated with the monsoon, it is still difficult to use ENSO-related SST to predict the monsoon because of the spring predictability barrier related to the low persistence of Pacific SST from winter to the next summer. We also confirm the relationship between IO SST and the

monsoon by examining the regression of MAM SST against the first EOF mode of JJA precipitation (figures not shown). The regression pattern bears large similarity to the SST pattern shown Figures 3 for MAM. Similar SST patterns are also obtained in the regression of MAM SST against the various JJA monsoon indices.

We also search for pairs of spatial patterns that explain maximum temporal covariance between the two fields using results from an SVD analysis for SST and precipitation. We follow Bretherton et al. [1992] and Wallace et al. [1992] and analyze the heterogeneous regression patterns of SVD modes. The heterogeneous patterns highlight the spatial features in one field (e.g., precipitation) that exhibit strong temporal relationships with the corresponding expansion coefficients of the other field (e.g., SST; also see Lau and Nath, 1994). Figure 8 shows the heterogeneous regression patterns for the first two SVD modes. The figure demonstrates the relationship between MAM SST and JJA precipitation (Figures 8a-b), and between SON SST and DJF precipitation (Figures 8c-d). In particular, the right panel of Figure 8a indicates how well the pattern of JJA precipitation can be specified or predicted from the expansion coefficient of SST associated with the MAM SST pattern in the left panel. Figure 8a indicates that the MAM SST is followed by an increase in precipitation over the equatorial-northern IO and southern Asia and a decrease in precipitation over the western Pacific and northern Southeast Asia. In the second mode (Figure 8b), the precipitation feature is dominated by strong increases in the longitudinal band of

90°E-150°E. It is noted that the SST patterns in Figure 8a are similar to the regression patterns shown in Figure 3b. Thus, the SVD analysis confirms the results presented in Figure 7c (for precipitation) and Table 3 for the relationship between MAM IO SST and the Asian summer monsoon.

For SON SST and DJF precipitation (Figures 8c-d), the first mode shows an out-of-phase change in precipitation to the west and east of 80°E, with two broad centers over the equatorial western IO and western Pacific. In the second mode, an out-of-phase precipitation feature appears to the west of 120°E, between the north and the south of 5°S. An apparent increase in precipitation can also be found over northern Australia. The SST and precipitation patterns shown here for the first mode are similar to those presented in Figure 3d (for SST) and Figure 7a (for precipitation).

We also perform a similar SVD analysis for the SST of northern (north of 10°S) and southern (south of 10°S) IO, respectively. Figure 9 shows the heterogeneous regression patterns of the first two SVD modes between JJA precipitation and the MAM SST of northern IO (Figures 9a-b) and southern IO (Figures 9c-d). Compared to the northern IO SST, the southern IO SST is associated with features of the Asian monsoon that are more similar to those shown in Figures 8a-b. In particular, the coefficient of pattern correlation for precipitation is 0.93 between Figure 9c and Figure 8a, but only 0.79 between Figure 9a and Figure 8a. A similar result also occurs in the second mode: the coefficient is 0.9 between Figure 9d and Figure 8b, but only 0.24 between Figure 9b and

Figure 8b.

The importance of southern IO SST for the Asian summer monsoon can also be seen from Figure 10, which shows the relationship of the monsoon with the first EOF modes of MAM SST over the northern and southern IO, respectively. The figure shows a large resemblance between Figure 7c (for the entire IO SST) and Figure 10b (for the southern IO SST), especially over the IO and western Pacific sector. The features shown in Figure 10b are clearly distinguished from those shown in Figure 10a (for the northern IO SST).

We also investigate the relative relationship of winter precipitation with the preceding SON SST of northern and southern IO (figures not shown). The northern IO SST accounts for a similar precipitation pattern in DJF including the Australian monsoon. However, the difference between the impacts of northern and southern IO mainly appears in the second SVD mode and is less significant than the difference between the influences of northern and southern IO MAM SSTs on the Asian summer monsoon.

6. Summary and further discussions

a. Summary

In this study, we have investigated the relationships between the Indian Ocean SST and regional climate including the Asian and Australian monsoons. We have focused on the dominant

features of IO SST, the impacts of IO SST on different monsoon components, and the relative importance of the northern and southern IO for the monsoons.

The dominant mode of IO SST is characterized by uniform warming or cooling, which exerts a larger impact on monsoon climate than the tropical IO dipole. The IO SST is also characterized by large persistence from the boreal fall to the following spring and summer, and a drop in persistence from summer to fall, different clearly from the NINO3 SST, which is marked by an abrupt reduction in persistence in spring. The large persistence of IO SST prior to the Asian summer monsoon provides a predictive potential of the monsoon. The IO SST leads to opposite changes in the South and Southeast Asian monsoons, reinforcing the out-of-phase relationship that often appears between the two components. While a warmer IO strengthens the SAM, it weakens the SEAM. The difference in the phase-locking of SST persistence relative to the annual cycle between IO and NINO3 SSTs also means a seasonal alternation of the dominance of ENSO-monsoon and IO-monsoon relationships and implies a difference in the seasonality of their climate impacts. Indeed, while the NINO3 SST exerts an apparently larger impact on the climate in the boreal winter and the transitional seasons, the IO SST affects the summer regional climate more strongly. Furthermore, the southern IO SST influences the Asian summer monsoon more significantly than the northern IO SST. The boreal fall IO SST, especially that in the north, is strongly associated with the subsequent Australian summer monsoon.

The current work is distinct from previous studies in several aspects. First, we have emphasized the importance of southern IO, where the largest variance of IO SST appears, for the variability of the Asian summer monsoon. In our analysis, we have included SST information of the extratropical southern IO. Second, we have devoted substantial efforts towards understanding the IO SST related signals in different monsoon components including the South Asian (Indian) monsoon, SEAM, EAM, broad-scale Asian monsoon circulation, and the Australian monsoon. The analysis is among the most comprehensive studies of the relationships between IO SST and monsoons, because it has depicted the IO-related changes in most of the major monsoon components of the AAS system and the differences between these changes and those due to the ENSO's impact. Third, we have investigated the relative importance of the northern and southern IO SSTs for the monsoon climate.

b. Discussions

In this study, we have revealed several features about the persistence of IO SST, the relative climate impacts of IO SST and Pacific SST, and the importance of southern IO for Asian monsoon variability. As shown in Figure 3, the IO SST is largely persistent from SON to the following summer but the persistence becomes small from JJA to SON due to the influence of Asian summer monsoon. This is clearly different from the evolution of NINO3 SST, which is

usually persistent from JJA to DJF but loses memory in springtime related partially to the abrupt development of the monsoon [Webster and Yang, 1992; Lau and Yang, 1996]. These phase-locking features of persistence of the IO and NINO3 SSTs explain the predictive potential of SON (MAM) IO SST for DJF Australian (JJA Asian) monsoon and highlight the impacts of JJA and DJF NINO3 SSTs on the climate of transitional seasons, as demonstrated in Figure 7 and Table 3.

Our results have also indicated that the southern IO SST more strongly influences the Asian summer monsoon than its northern IO counterpart. This feature appears consistently in various analyses including SVD, EOF, linear regression, and pattern correlation methods. We have also reproduced the results by using data in which the linear trends are removed, indicating that the linear trends of IO SST for the study period have no significant impact on the features revealed by this study.

The southern IO SST can affect the Asian monsoon in several ways. The change in the tropical and southern IO SST alters the broad-scale meridional temperature gradient. According to Yang et al. [2004], an increased meridional temperature gradient prior to the summer monsoon (associated with cooling in the Asian continent and warming in the tropical and southern IO) leads to intensification of the upper-tropospheric westerlies over subtropical Asia, particularly the Middle East jet stream. The intensified westerlies, usually accompanied by intrusion of large-scale troughs, cause more precipitation including snow and soil moisture and decrease land surface temperature.

As a result, lower-than-normal geopotential height appears over southern Asia, favoring a late and weak establishment of the South Asian High in late spring and Asian monsoon in summer. The effect of changing the meridional temperature gradient on the monsoon seems more appropriate for explaining the variability of large-scale monsoon circulation, as indicated by the change in WY index shown in Table 3 (also see Yang et al., 2004).

The anomalies of SST over the tropical IO are often linked to the variability of the local Indian monsoon because of the effects of latent heat and water vapor supply. For example, a warming in the IO leads to a strong Indian monsoon, an important feature usually applied in explaining the tropospheric biennial oscillation [Meehl, 1997; Chang and Li, 2000]. (Note the opposite-sign changes of the local Indian monsoon and the South Asian monsoon from the large-scale WY monsoon and the Southeast Asian monsoon as shown in Table 3.) Thus, an understanding of the maintenance of subtropical southern IO SST anomalies and their northward shift is helpful for explaining this influence of IO SST on the local Indian monsoon.

Previous studies [e.g., Annamalai et al., 2003; Li et al., 2003; Wang et al., 2003; Terray et al., 2005] have emphasized the importance of the interaction between SST and the overlying atmosphere and the effects of ENSO and the convection over the maritime continent in maintaining the anomalies of southern IO SST. For example, when the convection over the maritime continent decreases in SON, an anomalous anticyclonic pattern develops in the overlying atmosphere as a

Rossby wave response and positive SST anomalies appear underneath. This anticyclonic pattern weakens the basic flow over the tropical and subtropical southern IO and further maintains the positive SST anomalies until the basic flow changes its direction in late spring or early summer. Also, to the northeast of this anticyclone, the anomalous southeasterly flow is accompanied by convergence over the tropical IO, leading to an increase in precipitation. The freshwater input associated with the increased precipitation helps stabilize the upper ocean and increase the SST to the north of the anticyclone [Yang et al., 1999]. This process facilitates a northward “propagation” of the positive SST anomalies, which has also been noticed by Huang and Shukla, [2005]. The northward shift of the SST anomalies can also be associated with the seasonal transition from MAM to JJA.

The above discussion of southern IO SST on the local Indian monsoon is supported by an important feature shown in Figure 10b: the leading mode of MAM IO SST is related to an anomalous cyclonic circulation over the southeastern IO (to the west of Australia) and an anticyclonic circulation over its northwest in the boreal summer. These anomalous circulation patterns strengthen the southwesterly flow of the climatological anticyclonic circulation (see Fig. 2c) over the central southern IO and cause a northwestward shift of the Mascarene high. These features are associated with larger northward moisture transportation and more precipitation over the equatorial IO because of the convergence between the southeasterly-easterly flow of this

anticyclonic circulation and the southward anomalous flow from the northern IO (see Figure 10b).

The important role of southern IO SST in the variability of Asian monsoon has aroused only limited research interest during the recent years. Thus, the leading mechanisms responsible for the SST's impact on the monsoon have not been fully explored. To improve our understanding of these mechanisms, more studies with longer data records and reliable models are necessary.

Acknowledgments

The authors would like to acknowledge a number of helpful discussions with Drs. H. Annamalai, Kyu-Myong Kim, Raghu Murtugudde, Renguang Wu, Yan Xue, and Qin Zhang. They are thankful to Editor Dr. Ruth Lieberman and the three anonymous reviewers for many constructive comments, and to Dr. Tim Eichler of the NOAA's Office of Scientific Support and Dr. John Fasullo of the National Center for Atmospheric Research for helping improve the readability of the paper. The first author is thankful to NOAA's Climate Prediction Center for providing support when this work was conducted. Dr. Ho was supported by the Technical Development for Remote Sensing Meteorology project funded by the Korean Meteorological Administration.

References

- Alexander, M. A., I. Blade, M. Newman, J. R. Lanzante, N.-C. Lau, and J. D. Scott, The atmospheric bridge: The influence of ENSO teleconnections on air-sea interaction over the global oceans. *J. Climate*, **15**, 2205-2231, 2002.
- Allan, R., D. Chambers, W. Drosowsky, and Coauthors, Is there an Indian Ocean dipole, and is it independent of the El Niño-Southern Oscillation. *CLIVAR Exch.*, **6**, 18-22, 2001.
- An, S.-I., A dynamic link between the basin-scale and zonal modes in the tropical Indian Ocean. *Theor. Appl. Climatol.*, **78**, 203-215, 2004.
- Annamalai, H., R. Murtugudde, J. Potemra, S. Xie, P. Liu, and B. Wang, Coupled dynamics over the Indian Ocean: Spring initiation of the zonal mode. *Deep-Sea Res. Part II*, **50**, 2305-2330, 2003.
- Annamalai, H., S. Xie, J. P. McCreary, and R. Murtugudde, Impact of Indian Ocean sea surface temperature on developing El Niño. *J. Climate*, **18**, 302-319, 2005.
- Ashok, K., Z. Guan, and T. Yamagata, Impact of the Indian Ocean dipole on the decadal relationship between the Indian monsoon rainfall and ENSO. *Geophys. Res. Lett.*, **28**, 4499-4502, 2001.
- Ashok, K., Z. Guan, and T. Yamagata, Influence of the Indian Ocean dipole on the Australian winter rainfall. *Geophys. Res. Lett.*, **30**, doi: 10.1029/2003GL017926, 2003a.
- Ashok, K., Z. Guan, and T. Yamagata, A look at the relationship between the ENSO and the Indian Ocean dipole. *J. Meteorol. Soc. Jpn.*, **81**, 41-56, 2003b.
- Ashok, K., W. L. Chan, T. Motoi, and T. Yamagata, Decadal variability of the Indian Ocean dipole. *Geophys. Res. Lett.*, **31**, doi: 10.1029/2004GL021345, 2004a.
- Ashok, K., Z. Guan, N. H. Saji, and T. Yamagata, Individual and combined influences of ENSO and the Indian Ocean dipole on the Indian summer monsoon. *J. Climate*, **17**, 3141-3155, 2004b.
- Baquero-Bernal, A., M. Latif, and S. Legutke, On dipole like variability of sea surface temperature in the tropical Indian Ocean. *J. Climate*, **15**, 1358-1368, 2002.

- Behera, S. K., S. Krishnan, and T. Yamagata, Unusual ocean-atmosphere conditions in the tropical Indian Ocean during 1994, *Geophys. Res. Lett.*, **26**, 3001-3004, 1999.
- Behera, S. K., and T. Yamagata, Subtropical SST dipole events in the southern Indian Ocean. *Geophys. Res. Lett.*, **28**, 327-330, 2001.
- Behera, S. K., S. A. Rao, H. N. Saji, and T. Yamagata, Comments on “A cautionary note on the interpretation of EOFs”. *J. Climate*, **16**, 1087-1093, 2003.
- Bretherton, C. S., C. Smith, and J. M. Wallace, An intercomparison of methods for finding coupled patterns in climate data. *J. Climate*, **5**, 541-560, 1992.
- Chang, C.-P., and T. Li, A theory for the tropical tropospheric biennial oscillation. *J. Atmos. Sci.*, **57**, 2209-2224, 2000.
- Chen, T.-C., and M.-C. Yen, Interannual variation of the Indian monsoon simulated by the NCAR community climate model: Effect of the tropical Pacific SST. *J. Climate*, **7**, 1403-1415, 1994.
- Dommenget, D., and M. Latif, A cautionary note on the interpretation of EOF. *J. Climate*, **15**, 216-225, 2002.
- Drosowsky, W. and L. E. Chambers, Near-global sea surface temperature anomalies as predictors of Australian seasonal rainfall. *J. Climate*, **14**, 1677-1687, 2001.
- Druyan, L. M., J. R. Miller, and G. L. Russell, Atmospheric general circulation model simulations with an interactive ocean: Effects of sea surface temperature anomalies in the Arabian Sea. *Atmos.-Ocean*, **21**, 94-106, 1983.
- Fasullo, J., Biennial Characteristics of Indian monsoon rainfall. *J. Climate*, **17**, 2972-2982, 2004.
- Fischer, A. S., P. Terray, P. Delecluse, S. Gualdi, and E. Guilyardi, Triggers for tropical Indian Ocean variability and links to ENSO in a constrained coupled climate model. *J. Climate*, 2005 (submitted).
- Goddard, L., and N. E. Graham, Importance of the Indian Ocean for simulating rainfall anomalies over

- eastern and southern Africa. *J. Geophys. Res.*, **104**, 19099-19116, 1999.
- Goswami, B. N., B. Krishnamurthy, and H. Annamalai, A broad-scale circulation index for interannual variability of the Indian summer monsoon. *Quart. J. Roy. Meteorol. Soc.*, **125**, 611-633, 1999.
- Guan, Z., and T. Yamagata, The unusual summer of 1994 in east Asia: IOD teleconnections. *Geophys. Res. Lett.*, **30**, doi:10.1029/2002GL016831, 2003.
- Harzallah, A., and R. Sadourny, Observed lead-lag relationships between Indian summer monsoon and some meteorological variables. *Clim. Dyn.*, **13**, 635-648, 1997.
- Hu, Z.-Z., R. Wu, J. L. Kinter, and S. Yang, Connection of summer rainfall variations in South and East Asia: Role of ENSO. *Int. J. Climatol.*, **25**, 1279-1289, 2005.
- Huang, B., and J. Shukla, On the mechanisms of the interannual variability in the tropical Indian Ocean. Part II: regional processes. *COLA Tech. Rep.*, **177**, 42 pp., 2005.
- Kalnay, E., and Coauthors, The NCEP/NCAR 40-year reanalysis project. *Bull. Amer. Meteorol. Soc.*, **77**, 437-471, 1996.
- Kim, K.-M., and K.-M. Lau, Dynamics of monsoon-induced biennial variability in ENSO. *Geophys. Res. Lett.*, **28**, 315-318, 2001.
- Krishnamurthy, V., and B. P. Kirtman, Variability of the Indian Ocean: Relation to monsoon and ENSO. *Quart. J. Roy. Meteorol. Soc.*, **129**, 1623-1646, 2003.
- Lau, K.-M., and S. Yang, The Asian monsoon and predictability of the tropical ocean-atmosphere system. *Quart. J. Roy. Meteor. Soc.*, **122**, 945-957, 1996.
- Lau, K.-M., K.-M. Kim, and S. Yang, Dynamical and boundary forcing characteristics of regional components of the Asian summer monsoon. *J. Climate*, **13**, 2461-2482, 2000.
- Lau, N.-C., and M. J. Nath, A modeling study of the relative roles of tropical and extratropical SST anomalies in the variability of the global atmosphere-ocean system. *J. Climate*, **7**, 1184-1207, 1994.

- Lau, N.-C., and M. J. Nath, The role of the “atmospheric bridge” in linking tropical Pacific ENSO events to extratropical SST anomalies. *J. Climate*, **9**, 2036-2057, 1996.
- Lau, N.-C. and M. J. Nath, Coupled GCM simulation of atmosphere-ocean variability associated with zonally asymmetric SST changes in the tropical Indian Ocean. *J. Climate*, **17**, 245-265, 2004.
- Li, T., B. Wang, C. P. Chang, and Y. S. Zhang, A theory for the Indian Ocean dipole-zonal mode. *J. Atmos. Sci.*, **60**, 2119-2135, 2003.
- Mason, S. J., Sea-surface temperature-south African rainfall associations. 1910-1989. *Int. J. Climatol.*, **15**, 119-135, 1995.
- Meehl, G. A., The annual cycle and interannual variability in the tropical Pacific and Indian Ocean region. *Mon. Wea. Rev.*, **115**, 27-50, 1987.
- Meehl, G. A., The South Asian monsoon and the tropospheric biennial oscillation. *J. Climate*, **10**, 1921-1943, 1997.
- Meehl, G. A., and J. M. Arblaster, The tropospheric biennial oscillation and Asian-Australian monsoon rainfall. *J. Climate*, **15**, 722-744, 2002.
- Meehl, G. A., J. M. Arblaster, and J. Loschnigg, Coupled ocean-atmosphere dynamical processes in the tropical Indian and Pacific Oceans and the TBO. *J. Climate*, **16**, 2138-2158, 2003.
- Murtugudde, R., J. P. McCreary, and A. J. Busalacchi, Oceanic processes associated with anomalous events in the Indian Ocean with relevance to 1997-1998. *J. Geophys. Res.*, **105**, 3295-3306, 2000.
- Nicholls, N., Sea surface temperatures and Australian winter rainfall. *J. Climate*, **2**, 965-973, 1989.
- Nitta, T., and S. Yamada, Recent warming of tropical sea surface temperature and its relationship to the Northern Hemisphere circulation. *J. Meteorol. Soc. Jpn.*, **67**, 375-383, 1989.
- Palmer, T. N., C. Brankovic, P. Viterbo, and M. J. Miller, Modeling interannual variations of summer monsoons. *J. Climate*, **5**, 399-417, 1992.
- Parthasarathy, B., A. A. Munot, and D. R. Kothawale, Monthly and seasonal rainfall series for All-India

- homogeneous regions and meteorological subdivisions: 1987-1994. *Contributions from Indian Institute of Tropical Meteorology*, Research Report RR-065, Pune 411 008 INDIA, 1995.
- Peterson, R. G., and W. White, Slow oceanic teleconnections linking the Antarctic circumpolar wave with tropical ENSO. *J. Geophys. Res.*, **103**, 24, 573-24,583, 1998.
- Rao, K. G., and B. N. Goswami, Interannual variations in sea surface temperature of the Arabian sea and the Indian monsoon: A new perspective. *Mon. Wea. Rev.*, **116**, 558-568, 1988.
- Rao, S. A., S. K. Behera, Y. Masumoto, and T. Yamagata, Interannual variability in the subsurface tropical Indian Ocean. *Deep-Sea Research II*, **49**, 1549-1572, 2002.
- Reason, C. J. C., Warm and cold events in the southeast Atlantic/southwest Indian Ocean region and potential impacts on circulation and rainfall over southern Africa. *Meteorol. Atmos. Phys.*, **69**, 49-65, 1998.
- Reason, C. J. C., Subtropical Indian Ocean SST dipole events and southern African rainfall. *Geophys. Res. Lett.*, **28**, 2225-2227, 2001.
- Reason, C. J. C., Sensitivity of the southern African circulation to dipole sea-surface temperature patterns in the South Indian Ocean. *Int. J. Climatol.*, **22**, 377-393, 2002.
- Reynolds, R. W., N. A. Rayner, T. M. Smith, D. C. Stokes, and W. Wang, An improved in situ and satellite SST analysis for climate. *J. Climate*, **15**, 1609-1625, 2002.
- Saha, K., Zonal anomaly of sea surface temperature in equatorial Indian Ocean and its possible effect upon monsoon circulation. *Tellus*, **22**, 403-409, 1970.
- Saji, N. H., B. N. Goswami, P. N. Vinayachandran, and T. Yamagata, A dipole mode in the tropical Indian Ocean. *Nature*, **401**, 360-363, 1999.
- Saji, N. H., and T. Yamagata, Possible impacts of Indian Ocean dipole mode events on global climate. *Climate Res*, **25**, 151-169, 2003.
- Sarkar, S., R. P. Singh, and M. Kafatos, Further evidences for the weakening relationship of Indian rainfall

- and ENSO over India. *Geophys. Res. Lett.*, **31**, doi:10.1029/2004GL019848, 2004.
- Shinoda, T., H. H. Hendon, and M. A. Alexander, Surface and subsurface dipole variability in the Indian Ocean and its relation with ENSO. *Deep-Sea Research, Part I*, **51**, 619-635, 2004.
- Shukla, J., Effect of Arabian Sea surface temperature anomaly on Indian summer monsoon: A numerical experiment with the GFDL model. *J. Atmos. Sci.*, **32**, 503-511, 1975.
- Shukla, J. and B.M. Misra, Relationships between sea surface temperature and wind speed over the central Arabian Sea, and monsoon rainfall over India. *Mon. Wea. Rev.*, **105**, 998-1002, 1977.
- Tao, S., and L. Chen, A review of recent research on East Asian monsoon in China. *Monsoon Meteorology* (Eds. C.-P. Chang and T. N. Krishnamurti), Oxford University Press, London, 60-92, 1987.
- Terray, P., P. Delecluse, S. Labattu, and L. Terray, Sea surface temperature associations with the late Indian summer monsoon. *Clim. Dyn.*, **21**, 593-618, 2003.
- Terray, P., S. Dominiak, P. Delecluse, Role of the southern Indian Ocean in the transitions of the monsoon-ENSO system during recent decades. *Clim. Dyn.*, **24**, 169-195, 2005.
- Wallace, J. M., C. Smith, and C. S. Bretherton, Singular value decomposition of wintertime sea surface temperature and 500-mb height anomalies. *J. Climate*, **5**, 561-576, 1992.
- Wang, B., and Z. Fan, Choice of south Asian summer monsoon indices. *Bull. Amer. Meteor. Soc.*, **80**, 629-638, 1999.
- Wang, B., R. Wu, and T. Li, Atmosphere-warm ocean interaction and its impact on Asian-Australian monsoon variation. *J. Climate*, **16**, 1195-1211, 2003.
- Webster, P. J., and S. Yang, Monsoon and ENSO: Selectively interactive systems. *Quart. J. Roy. Meteor. Soc.*, **118**, 877-926, 1992.
- Webster, P. J., A. M. Moore, J. P. Loschnigg, and R. R. Leben, Coupled ocean-atmosphere dynamics in the Indian Ocean during 1997-98. *Nature*, **401**, 356-360, 1999.
- White, W., and R. G. Peterson, An Antarctic circumpolar wave in surface pressure, wind, temperature, and

- sea ice extent. *Nature*, **380**, 699-702, 1996.
- Xie, P., and P. A. Arkin, Analyses of global monthly precipitation using gauge observations, satellite estimates, and numerical model predictions. *J. Climate*, **9**, 840-858, 1996.
- Xie, S.-P., H. Annamalai, F. A. Schott, and J. P. McCreary, Structure and mechanism of south Indian Ocean climate variability. *J. Climate*, **15**, 864-878, 2002.
- Yamagata, T., S. K. Behera, S. A. Rao, Z. Guan, K. Ashok, and H. N. Saji, The Indian Ocean dipole: a physical entity. *Clivar Exchanges*, **24**, pp 15-18, 20-22, 2002.
- Yang, S., K.-M. Lau, and P. S. Schopf, The role of atmospheric hydrological forcing in coupled ocean-atmosphere system. *Climate Dyn*, **15**, 737-750, 1999.
- Yang, S., K. M. Lau, and K.-M. Kim, Variations of the East Asian jet stream and Asian-Pacific-American winter climate anomalies. *J. Climate*, **15**: 306-325, 2002.
- Yang, S., K.-M. Lau, S.-H. Yoo, J. L. Kinter, K. Miyakoda, and C.-H. Ho, Upstream subtropical signals preceding the Asian summer monsoon circulation. *J. Climate*, **17**, 4213-4229, 2004.
- Yu, J.-Y., S.-P. Weng, and J. D. Farrara, Ocean roles in the TBO transitions of the Indian-Australian monsoon system. *J. Climate*, **16**, 3072-3080, 2003.
- Yu, J.-Y., and K.-M. Lau, Contrasting Indian Ocean SST variability with and without ENSO influence: A coupled atmosphere-ocean GCM study. *Meteor. Atmos. Phys.*, DOI: 10.1007/s00703-004-0094-7, 2004.
- Zhu, Y. L., and D. D. Houghton, The impact of Indian Ocean SST on the large-scale Asian summer monsoon and the hydrological cycle. *Int. J. Climatol.*, **16**, 617-632, 1996.

Table captions

Table 1. Definitions of monsoon and SST indices.

Table 2. Simultaneous correlation between the principle components of the first two EOF modes of IO SST and climate indices including NINO3 SST, IOD, SDP, and various monsoon components. Only the values exceeding the 95% confidence level are shown.

Table 3. Lagged correlation between JJA Asian monsoon components and the EOF1 of previous MAM IO SST, and between DJF Australian monsoon (AuM) and the EOF1 of preceding SON IO SST. Values exceeding significantly the 95% confidence level are highlighted.

Figure captions

Figure 1. Climatology (shadings) and tendency (contours) of SST for DJF (a), MAM (b), JJA (c), and SON (d) for 1981-2005. The tendency represents the SST of the stated season minus that of the previous season. For example, the DJF tendency represents DJF-SON. Units are °C.

Figure 2. Climatology of 850-mb winds (vectors; in ms^{-1}) and standard deviation of seasonal mean SST (shadings) for DJF (a), MAM (b), JJA (c), and SON (d).

Figure 3. Regression (°C) of grid-point SST against the principle component of EOF1 for each season for DJF (a), MAM (b), JJA (c), and SON (d). Values shown in the parentheses indicate the percentage of SST variance explained by EOF1. The numbers by the filled (non-filled) arrows measure the correlation between IO SST of a specific season and the IO SST (NINO3 SST) of the preceding season. Only the values that significantly exceed the 95% confidence level are shown.

Figure 4. Regression of 850-mb winds (vectors) and precipitation (shadings) against the principle component of EOF1 (PC1) for each season. Values exceeding the 95% (90%) confidence level are shaded for winds (precipitation).

Figure 5. DJF Regression of 850-mb winds (vectors) and precipitation (shadings) against (a) NINO3 SST, (b) IOD, (c) SDP, and (d) Australian monsoon. Values exceeding the 95%

confidence level are shaded.

Figure 6. JJA Regression of 850-mb winds (vectors) and precipitation (shadings) against (a) WY monsoon index and (b) SEAM. Values exceeding the 95% confidence level are shaded.

Figure 7. Lagged regression of 850-mb winds and precipitation against the previous-season IO SST (a-d) and NINO3 SST (e-h) for each season. Values exceeding the 95% confidence level are shaded.

Figure 8. Heterogeneous regression patterns of the first and second SVD modes between MAM IO SST and subsequent JJA precipitation (a-b), and between SON IO SST and subsequent DJF precipitation (c-d). Values shown in the parentheses indicate the percentage of SST-precipitation covariance explained by the individual modes.

Figure 9. Heterogeneous regression patterns of the first and second SVD modes between MAM northern (north of 10°S) IO SST and subsequent JJA precipitation (a-b), and between MAM southern (south of 10°S) IO SST and JJA precipitation (c-d). Values shown in the parentheses indicate the percentage of SST-precipitation covariance explained by the individual modes.

Figure 10. Regression of JJA 850-mb winds and precipitation against the previous MAM PC1 of northern (a) and southern (b) IO SST. Values exceeding the 90% confidence level are shaded.

Table 1. Definitions of monsoon and SST indices.

Index	Definition
AIMR	Seasonally averaged precipitation over all Indian subdivisions from June to September
WY	Vertical zonal wind shear between 850 and 200 hPa, $U_{850}-U_{200}$, averaged over south Asia region ($5^{\circ}-20^{\circ}\text{N}/40^{\circ}-110^{\circ}\text{E}$) from June to August
SAM	Vertical meridional wind shear between 850 and 200 hPa, $V_{850}-V_{200}$, averaged over south Asia monsoon region ($10^{\circ}-30^{\circ}\text{N}/70^{\circ}-110^{\circ}\text{E}$) from June to August
SEAM	Horizontal zonal wind shear over the southeast Asia monsoon regions, U_{850} ($5^{\circ}-15^{\circ}\text{N}/90^{\circ}-130^{\circ}\text{E}$)- U_{850} ($22.5^{\circ}-32.5^{\circ}\text{N}/110^{\circ}-140^{\circ}\text{E}$), from June to August
EAM	Horizontal zonal wind shear over the east -southeast Asia monsoon regions, U_{200} ($25^{\circ}-35^{\circ}\text{N}/110^{\circ}-150^{\circ}\text{E}$)- U_{200} ($40^{\circ}-50^{\circ}\text{N}/110^{\circ}-150^{\circ}\text{E}$), from June to August
Australian Monsoon	Area averaged precipitation over Australian monsoon region ($20^{\circ}\text{S}-5^{\circ}\text{N}/100^{\circ}-150^{\circ}\text{E}$) from December to February
NINO3 SST	Area averaged SST over eastern Pacific region ($5^{\circ}\text{S}-5^{\circ}\text{N}/90^{\circ}-150^{\circ}\text{W}$)
IOD	Difference between area averaged SST over the western IO ($10^{\circ}\text{S}-10^{\circ}\text{N}/50^{\circ}-70^{\circ}\text{E}$) and the eastern IO ($10^{\circ}\text{S}-\text{Eq.}/90^{\circ}-110^{\circ}\text{E}$)
SDP	Difference between area averaged SST over the western IO ($37.5^{\circ}-27.5^{\circ}\text{S}/55^{\circ}-65^{\circ}\text{E}$) and the eastern IO ($28^{\circ}-18^{\circ}\text{S}/90^{\circ}-100^{\circ}\text{E}$)

Table 2. Simultaneous correlation between the principle components of the first two EOF modes of IO SST and climate indices including NINO3 SST, WY monsoon, AIMR, SAM, SEAM, EAM, Australian monsoon, IOD, and SDP. Only the values exceeding the 95% confidence level are shown in the table.

	EOF1	EOF2	IOD
DJF	NINO3 SST (0.55) IOD (0.41) SDP (-0.59) Australian Monsoon (-0.40)	SDP (-0.62)	
MAM	SDP (-0.60)	IOD (-0.49) SDP (-0.71)	SDP (0.59)
JJA	WY (-0.52) SEAM (-0.57)	IOD (-0.52) SDP (-0.65)	NINO3 SST (0.43)
SON	NINO3 SST (0.70) IOD (0.78)	IOD (-0.58) SDP (0.49)	NINO3 SST (0.76) SDP (-0.50)

Table 3. Lagged correlation between the JJA Asian monsoon and the EOF1 of previous MAM IO SST, and between the DJF Australian monsoon (AuM) and the EOF1 of preceding SON IO SST. The Asian monsoon components include AIMR, Webster-Yang (WY) broad-scale monsoon, SAM, EAM, and SEAM. Values exceeding the 95% confidence level are highlighted.

	JJA						DJF
	AIMR	WY	SAM	EAM	SEAM		AuM
MAM PC1	0.40	-0.34	0.47	0.02	-0.64	SON PC1	-0.49

SST Climatology and Tendency

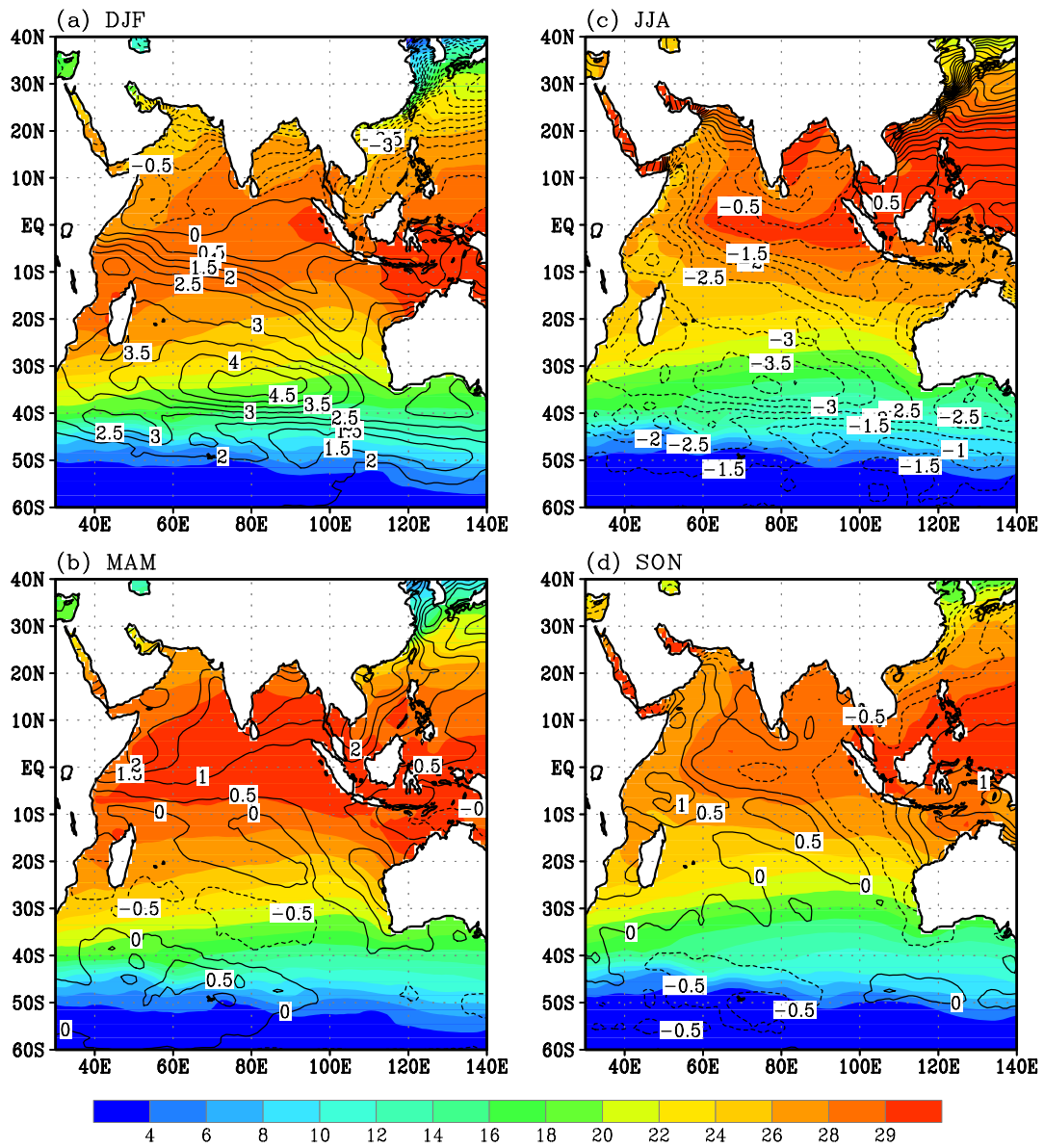


Figure 1. Climatology (shadings) and tendency (contours) of SST for DJF (a), MAM (b), JJA (c), and SON (d) for 1981-2005. The tendency represents the SST of the stated season minus that of the previous season. For example, the DJF tendency represents DJF-SON. Units are °C.

SST Standard Deviation and 850-mb Winds

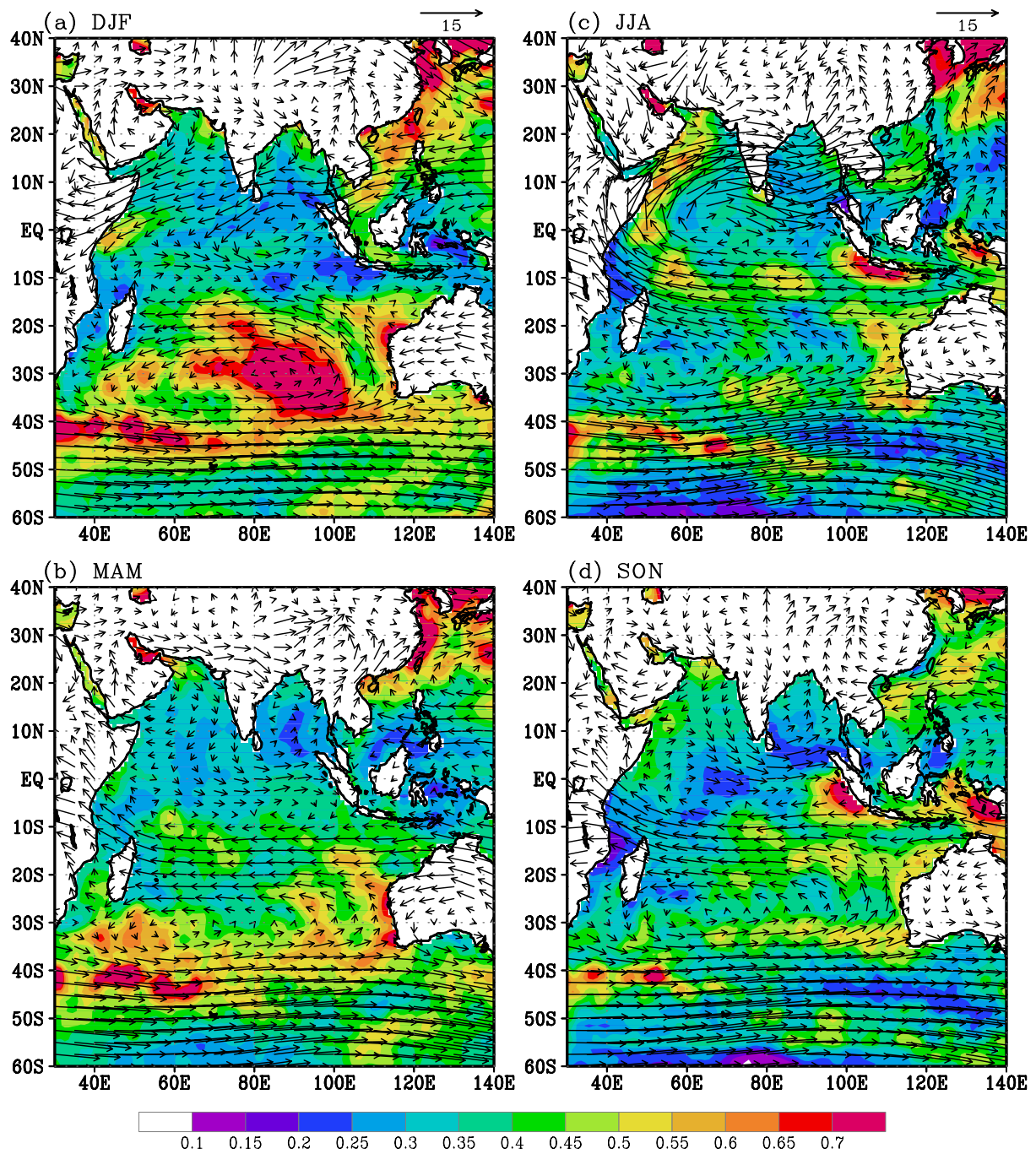


Figure 2. Climatology of 850-mb winds (vectors; in ms^{-1}) and standard deviation of seasonal mean SST (shadings) for DJF (a), MAM (b), JJA (c), and SON (d).

Regression of Grid-SST Against IO SST PC1

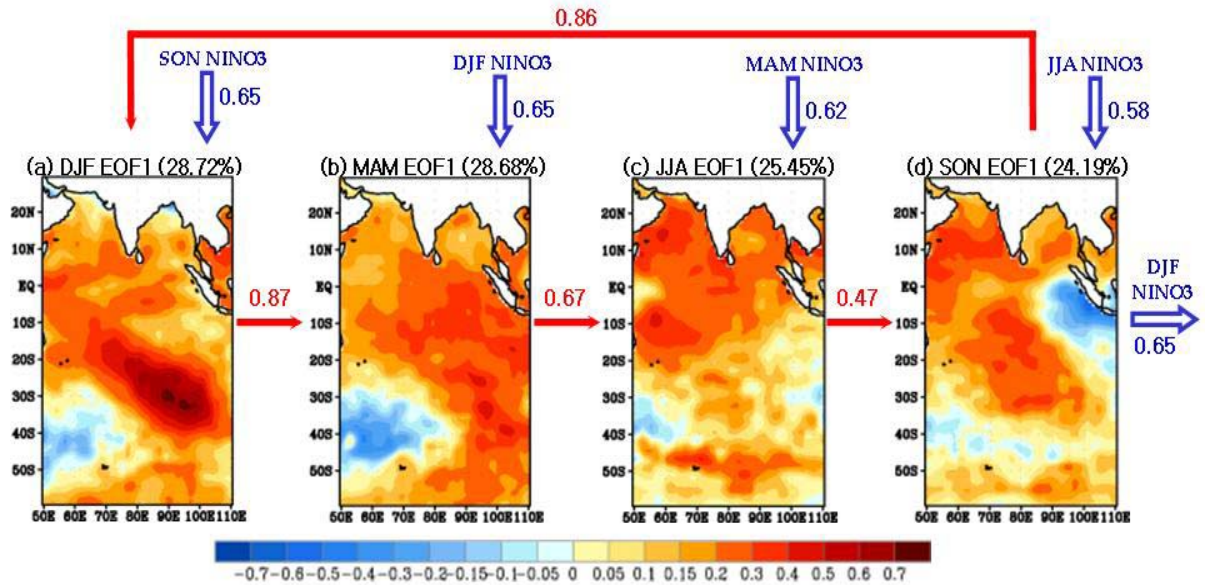


Figure 3. Regression ($^{\circ}\text{C}$) of grid-point SST against the principle component of EOF1 for each season for DJF (a), MAM (b), JJA (c), and SON (d). Values shown in the parentheses indicate the percentage of SST variance explained by EOF1. The numbers by the filled (non-filled) arrows measure the correlation between IO SST of a specific season and the IO SST (NINO3 SST) of the preceding season. Only the values that significantly exceed the 95% confidence level are shown.

Regression of Wind 850 & Precip against Leading PCs

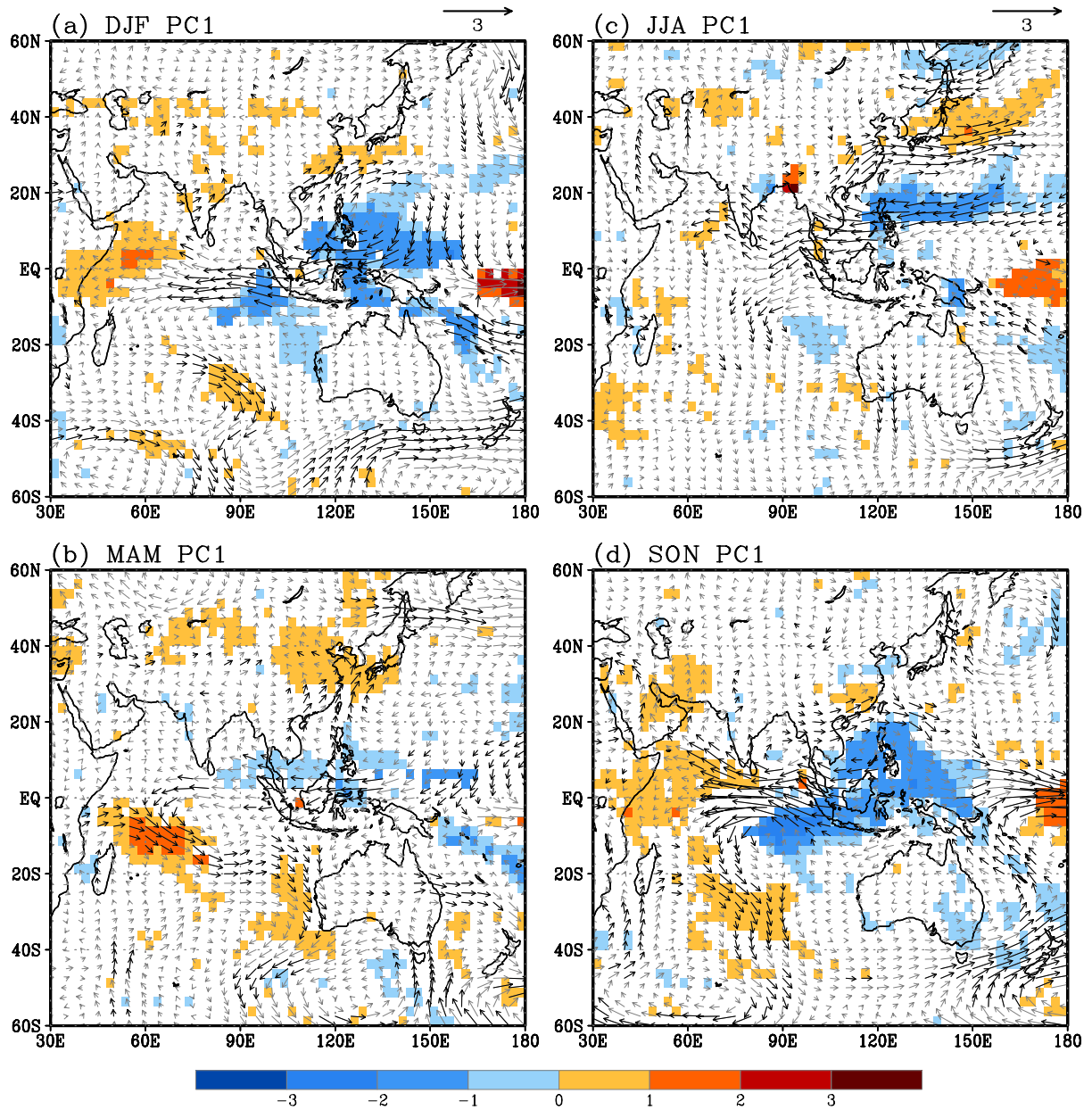


Figure 4. Regression of 850-mb winds (vectors) and precipitation (shadings) against the principle component of EOF1 (PC1) for each season. Values exceeding the 95% (90%) confidence level are shaded for winds (precipitation).

DJF Regression of 850-mb Winds & Precip against Climate Indices

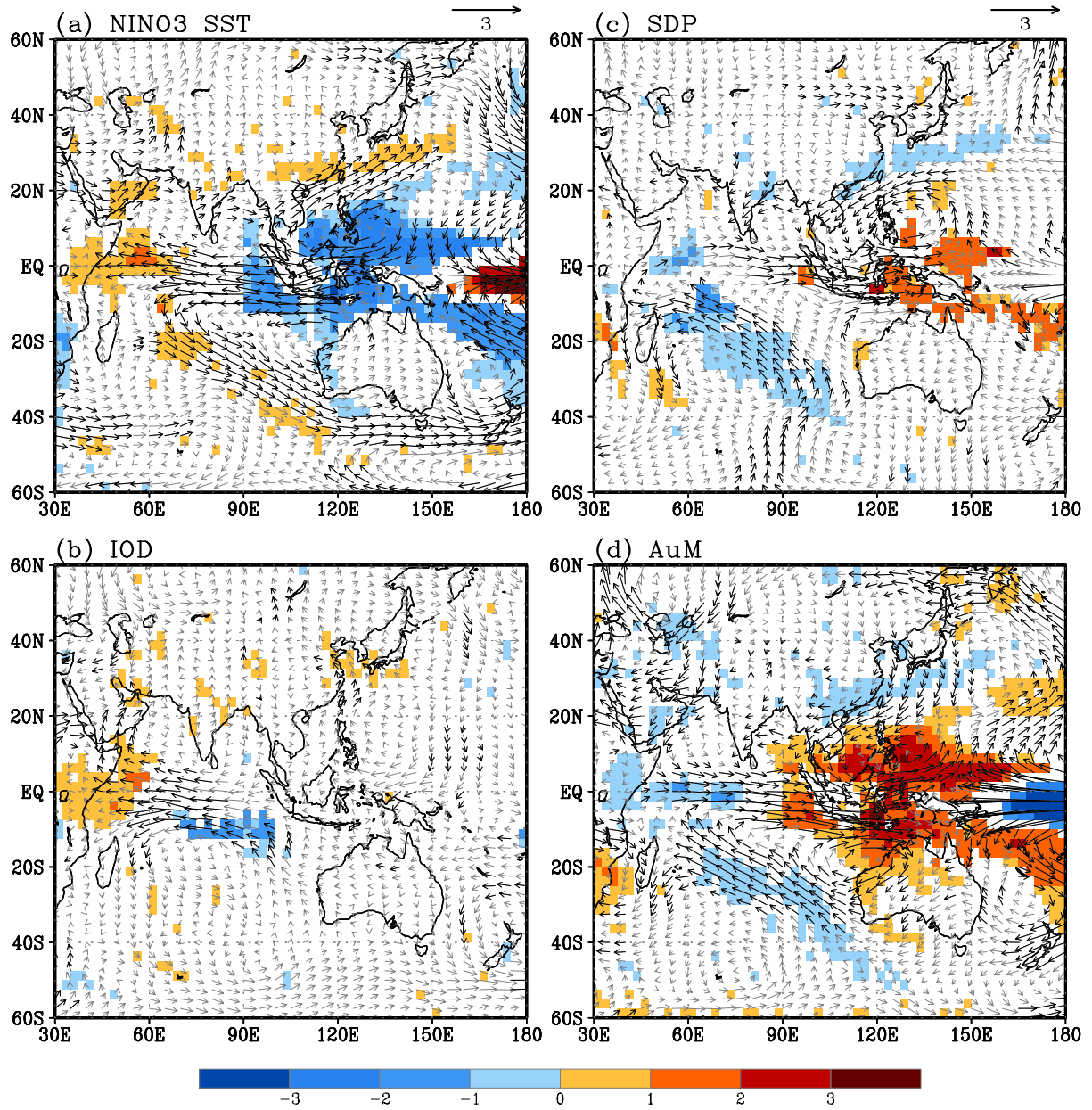


Figure 5. DJF Regression of 850-mb winds (vectors) and precipitation (shadings) against (a) NINO3 SST, (b) IOD, (c) SDP, and (d) Australian monsoon. Values exceeding the 95% confidence level are shaded.

JJA Regression of 850-mb Winds & Precip against Monsoon Indices

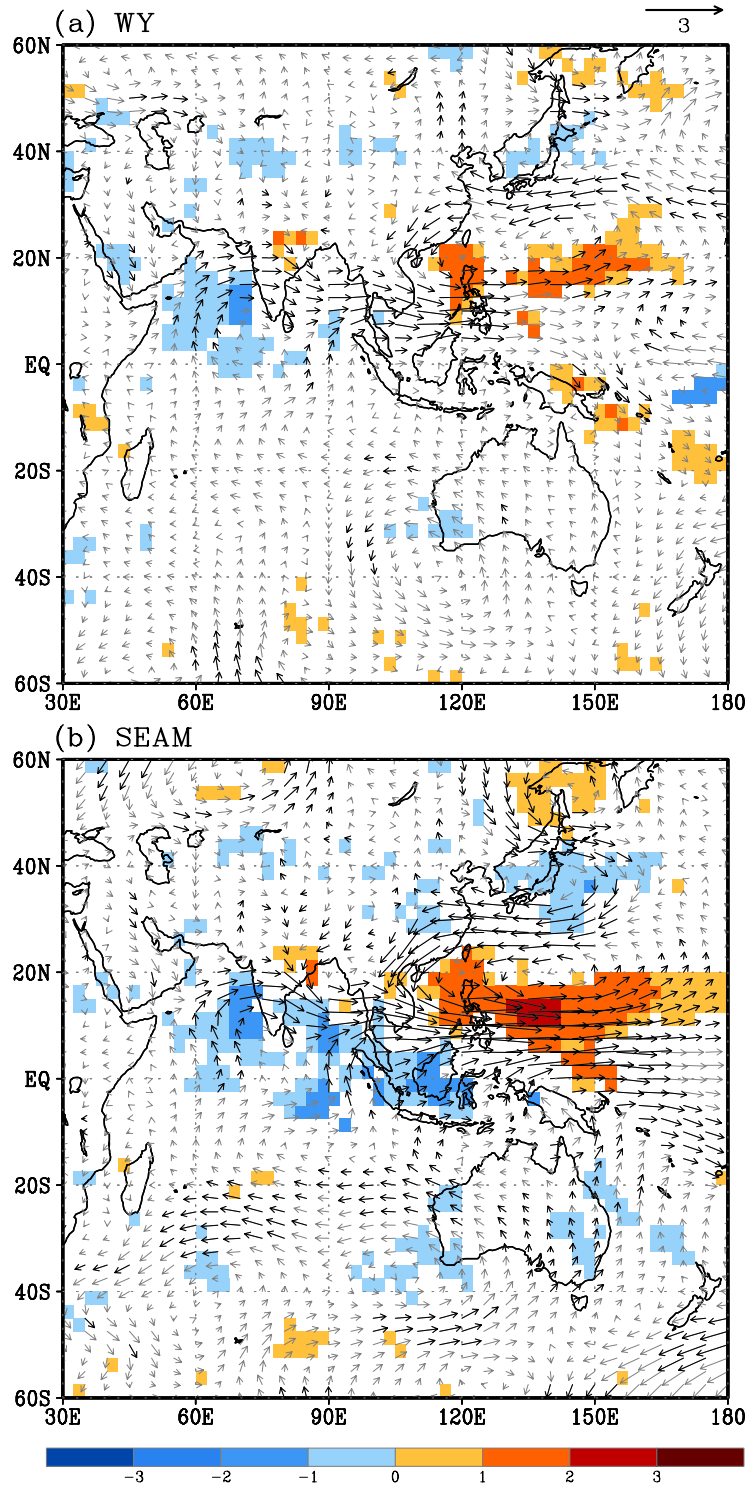


Figure 6. JJA Regression of 850-mb winds (vectors) and precipitation (shadings) against (a) WY monsoon index and (b) SEAM. Values exceeding the 95% confidence level are shaded.

Reg. of 850-mb Winds & Precip against NINO3 & IO SST Indices

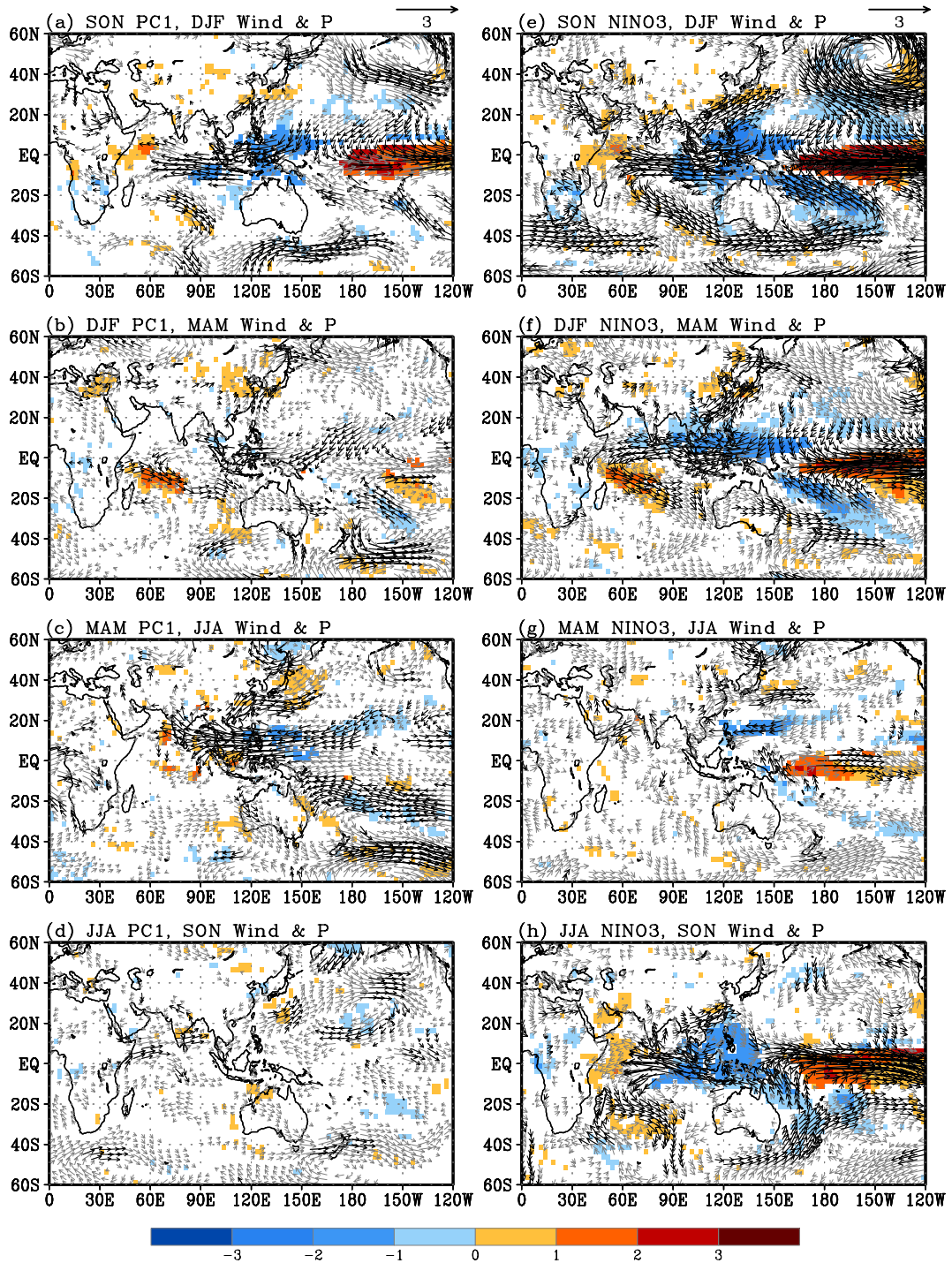
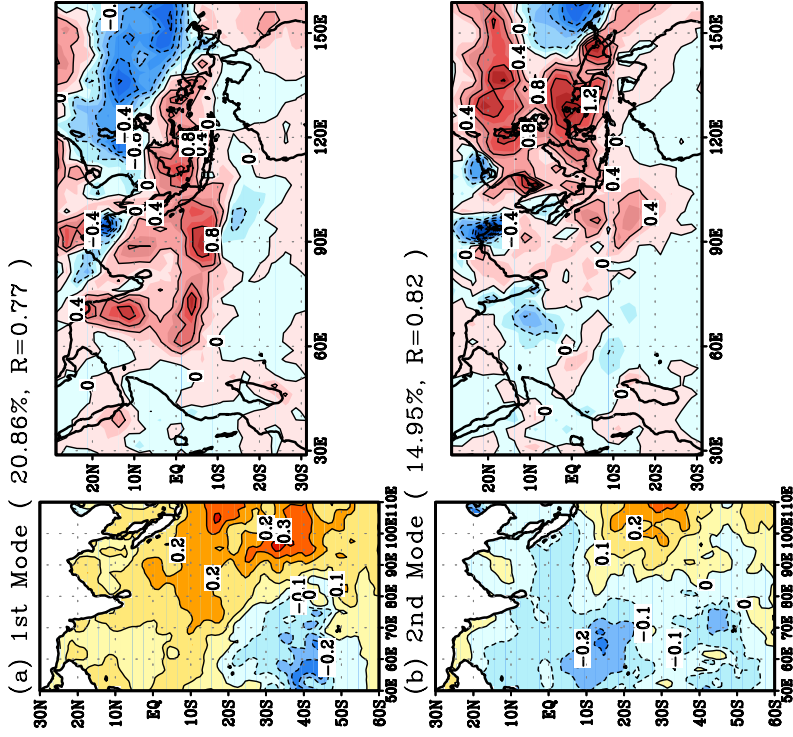


Figure 7. Lagged regression of 850-mb winds and precipitation against the previous-season IO SST (a-d) and NINO3 SST (e-h) for each season. Values exceeding the 95% confidence level are shaded.

Heterogeneous Reg. Patterns for SVD Modes between IOSST and Precip

[MAM SST & JJA P]



[SON SST & DJF P]

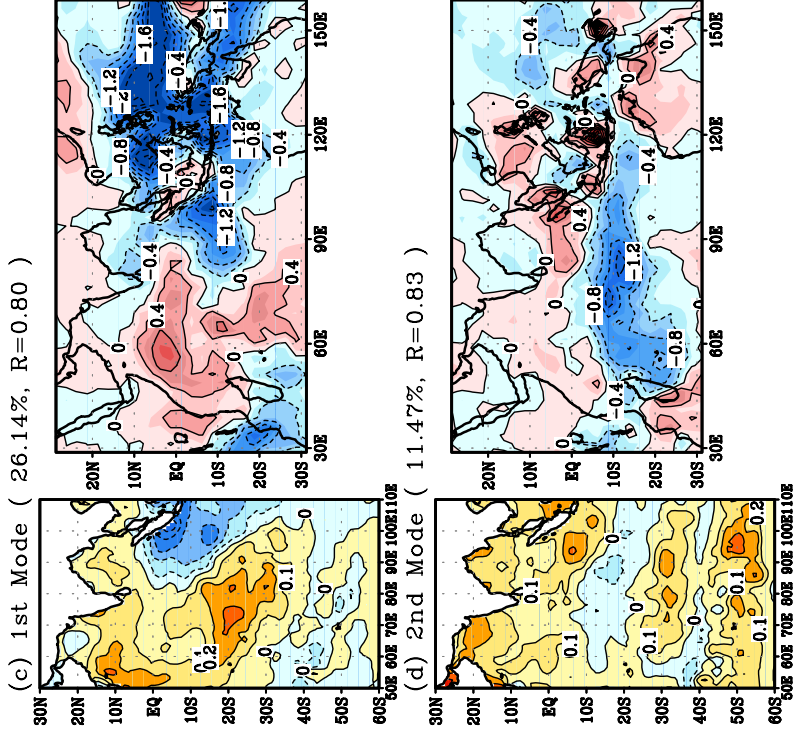


Figure 8. Heterogeneous regression patterns of the first and second SVD modes between MAM IO SST and subsequent JJA precipitation (a-b), and between SON IO SST and subsequent DJF precipitation (c-d). Values shown in the parentheses indicate the percentage of SST-precipitation covariance explained by the individual modes.

Hetero. Reg. Patterns for SVD Modes between MAM SST and JJA Precip

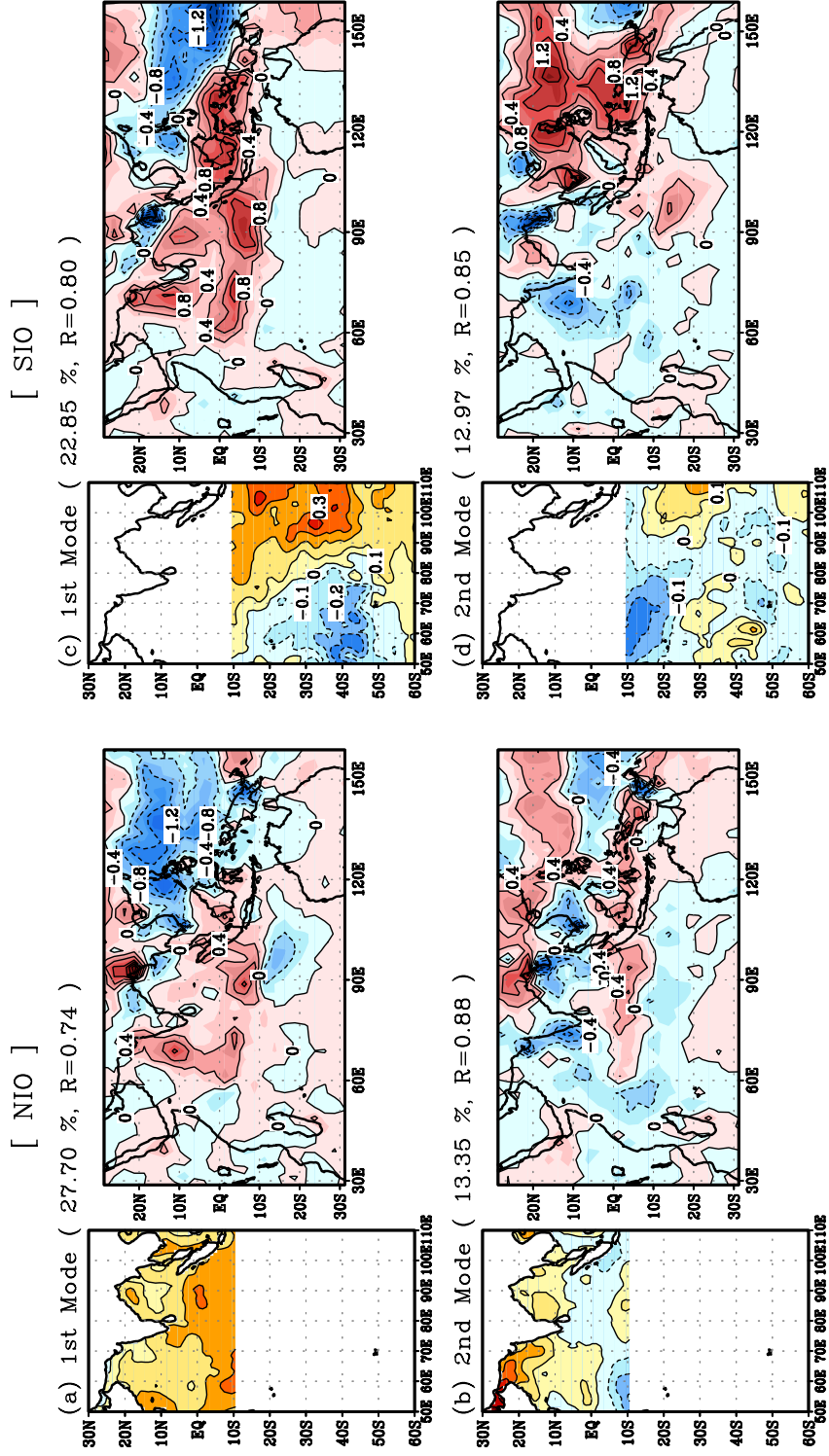


Figure 9. Heterogeneous regression patterns of the first and second SVD modes between MAM northern (north of 10°S) IO SST and subsequent JJA precipitation (a-b), and between MAM southern (south of 10°S) IO SST and JJA precipitation (c-d). Values shown in the parentheses indicate the percentage of SST-precipitation covariance explained by the individual modes.

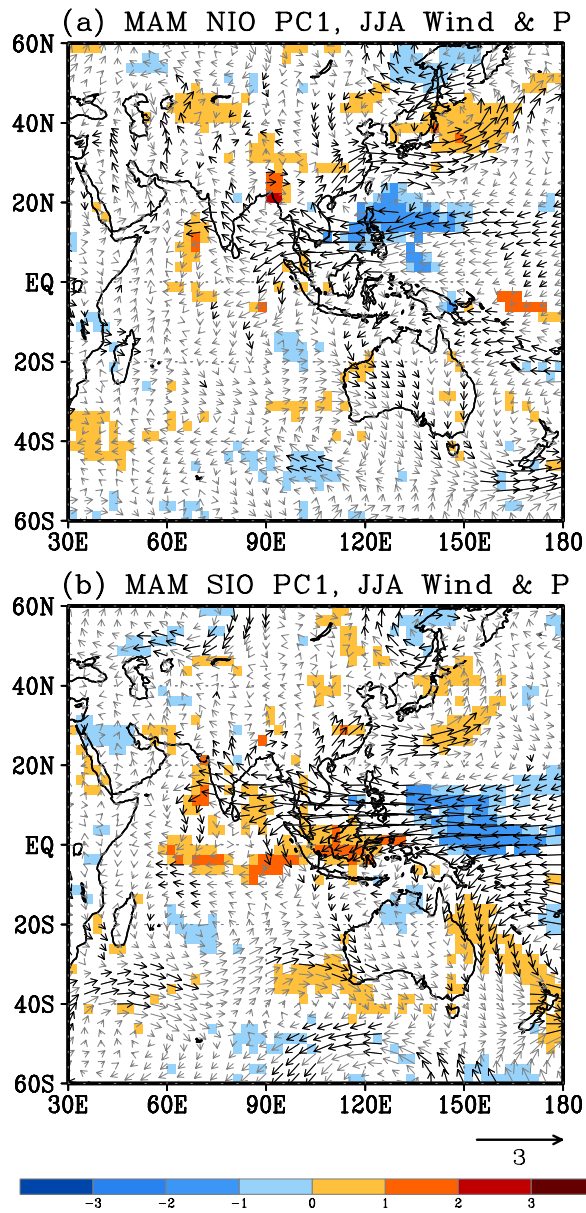


Figure 10. Regression of JJA 850-mb winds and precipitation against the previous MAM PC1 of northern (a) and southern (b) IO SST. Values exceeding the 90% confidence level are shaded.